A Study of Two High Intensity Fires across Corsican Shrubland

Jacky Fayad, Morandini Frédéric, Gilbert Accary, François-Joseph Chatelon, Clément Wandon, Antoine Burglin, Lucile Rossi, Thierry Marcelli, Dominique Cancellieri, Valérie Cancellieri, et al.

atmosphere

MDPI

Article

A Study of Two High Intensity Fires across Corsican Shrubland

Jacky Fayad [1,*], Frédéric Morandini [1], Gilbert Accary [2], François-Joseph Chatelon [1], Clément Wandon [1], Antoine Burglin [1], Lucile Rossi [1], Thierry Marcelli [1], Dominique Cancellieri [1], Valérie Cancellieri [1], Dominique Morvan [3], Sofiane Meradji [4], Antoine Pieri [1], Gilles Planelles [5], René Costantini [6], Patrice Briot [7] and Jean-Louis Rossi [1]

[1] Le Laboratoire Sciences Pour l'Environnement (UMR CNRS SPE 6134), Université de Corse, 20250 Corte, France
[2] Scientific Research Center in Engineering, Lebanese University, Museum Square, Beirut 1106, Lebanon
[3] M2P2, Centrale Marseille, CNRS, Aix-Marseille Université, 13451 Marseille, France
[4] IMATH Laboratory, EA 2134, Toulon University, 83160 Toulon, France
[5] Office National des Forêt–Corse-Unité Production Travaux-Responsable UP, 20000 Ajaccio, France
[6] SIS2B, Centre Administratif du Fango, 20200 Bastia, France
[7] Service Régional Ingénierie DFCI FORSAP de la Collectivité de Corse, 20187 Ajaccio, France
* Correspondence: fayad_j@univ-corse.fr; Tel.: +33-07-66602364

Abstract: This paper reports two experimental fires conducted at field-scale in Corsica, across a particular mountain shrubland. The orientation of the experimental plots was chosen in such a way that the wind was aligned along the main slope direction in order to obtain a high intensity fire. The first objective was to study the high intensity fire behavior by evaluating the propagation conditions related to its speed and intensity, as well as the geometry of the fire front and its impact on different targets. Therefore, an experimental protocol was designed to determine the properties of the fire spread using UAV cameras and its impact using heat flux gauges. Another objective was to study these experiments numerically using a fully physical fire model, namely FireStar3D. Numerical results concerning the fire dynamics, particularly the ROS, were also compared to other predictions of the FireStar2D model. The comparison with experimental measurements showed the robustness of the 3D approach with a maximum difference of 5.2% for the head fire ROS. The fire intensities obtained revealed that these experiments are representative of high intensity fires, which are very difficult to control in the case of real wildfires. Other parameters investigated numerically (flame geometry and heat fluxes) were also in fairly good agreement with the experimental measurements and confirm the capacity of FireStar3D to predict surface fires of high intensity.

Keywords: field experiment; fire behavior; high intensity fire; physical fire model

Citation: Fayad, J.; Morandini, F.; Accary, G.; Chatelon, F.-J.; Wandon, C.; Burglin, A.; Rossi, L.; Marcelli, T.; Cancellieri, D.; Cancellieri, V.; et al. A Study of Two High Intensity Fires across Corsican Shrubland. *Atmosphere* **2023**, *14*, 473. https://doi.org/10.3390/atmos14030473

Academic Editor: Kyu-Myong Kim

Received: 19 January 2023
Revised: 21 February 2023
Accepted: 24 February 2023
Published: 27 February 2023

1. Introduction

Wildfires are part of Mediterranean ecosystems and societies, where small scale fires may always be expected as a part of the management of natural resources. However, the occurrence of large-scale wildfires has dramatically increased throughout the region during the last decades, especially in European Mediterranean countries [1]. Thus, forest fires have become an extremely serious environmental issue with huge social, economic and environmental costs.

There are many complex reasons for the increase in wildfire hazard and risk. Climate change, changing cultural traditions such as rural depopulation, urban expansion and leisure behaviors, and sub-optimal fire management policies have all influenced the activities and impact of wildfires [2].

Regions around the Mediterranean Sea are considered prone to climate change [3]. In recent decades, Mediterranean climate regions have experienced frequent heat waves and tend to be warmer and drier [4,5], with a longer wildfire season. For example, in 2019 and 2020, the wildfire season was extended longer than expected in European regions, with

the number of burned areas and fires higher than the average of the last twelve years [2]. For the next century, severe droughts are expected to become more frequent, with global temperatures warmer than the current levels [2].

Climate change is also a growing concern as a driver of extreme wildfire events [6]. Consequently, the last years have witnessed many high intensity forest fires that have resulted in significant human and economic damages, making them potential catastrophes. For instance, Portugal (2005, 2017), Spain (2017), Greece (2017, 2018), Australia (2020), California (2021), and France (2022) are examples of places with high intensity forest fire incidents, among a non-exhaustive list [7–10]. As mentioned above, while climate change affects the frequency and intensity of wildfires, these events contribute themselves to climate change due to carbon emissions. According to the European Copernicus program, the forest fires that have ravaged Europe in recent months have resulted in very high greenhouse gas emissions; these fires emitted 6.4 megatons of carbon between 1 June and 3 August, a level that had not been reached for fifteen years [11].

Extreme wildfires are dangerous not only because of their impact on people, climate, and ecosystems: they are also unpredictable and uncontrollable [12]. These fires are characterized by a sudden change in fire behavior, spotting activities, and high rates of spread and fireline intensities. These fire characteristics can have major impacts on people and assets. Another criterion to define these wildfires events is the capacity of control that strongly depends on fire behavior, especially the fireline intensity. Thus, several rules have been developed to relate suppression effectiveness to fire intensity [13], in order to establish many categories according to the capacity of fire control [13–15]. For instance, a surface fire propagating across shrubland, grassland or forest, with an intensity lower than 2 MW/m is moderately difficult to control, while between 4 and 10 MW/m it becomes very difficult, or extremely difficult, especially when the flame lengths range between 3.5 and 10 m. In this case, any attempt to contain the fire's head may fail. However, for a fire intensity that exceeds 10 MW/m, especially for crown fire types, an extreme uncontrollable fire behavior takes place. In this case, the direct attack of the fire front (even with aerial means) becomes inefficient until the atmospheric conditions become less severe: with a lower air temperature level, a higher relative air humidity, and a lower wind velocity.

As high intensity fires could occur more frequently nowadays, their suppression requires good knowledge and measurements of the physical parameters governing their behavior, especially at field-scale. Knowing that suppression efforts can reach their limits of effectiveness, it should be required to redirect effort towards prevention measures based on fuel treatments and the integration of strategies and techniques that include prescribed fires, in order to shift from suppression to prevention. However, local measurements are still very useful for observing and understanding the macroscopic fire behavior, and also for comparing these measurements and data with the predictions of fully physical fire models.

A wide variety of experimental fires are present in the literature. At laboratory scale where propagation conditions are often well managed, it is therefore possible to repeat the experiments with several trials. The main objectives of these experiments are to develop propagation models through correlations based on the results obtained [16] or to compare these results with existing models [17–19]. These experiments also allow researchers to study the effect of different parameters (fuel moisture content, wind, slope, fuel characteristics) on fire behavior or flame geometry [20–23]. However, laboratory experimental fires may have certain limitations in terms of propagation conditions or fuel types, making their behavior different than real field fires.

At the field-scale, experimental programs with multiple objectives and issues have been conducted across a variety of fuel types and under different meteorological and topographical conditions. For instance, experimental fires have been carried out in order to establish mathematical correlations and propagation models related to several physical parameters, through different vegetation types, grassland [24,25], and shrubland [26–28]. Other studies carried out on different shrubland fuel loads have allowed the analysis of

the fire front behavior and geometry across sloping terrain, and also the measurement of radiative and total heat transfer during propagation [29,30]; Bulter et al. [31] have reported the fire rates of spread of low-intensity fires spreading in longleaf pine. Viegas et al. [32] experimentally investigated junction fires, at laboratory and small field cases, where these results were compared also to a previous wildfire; later on, this kind of fire was reproduced numerically using CFD-based numerical models [33].

The purpose of citing these previous studies is to show that considerable progress has been made in the characterization and understanding of wildland fire behavior. However, most of these studies are conducted at small scale, or on small plots with no or moderate slopes or wind speeds, consequently resulting in low intensity fires. This may be due to the fact that experimental field-scale fires are problematic in terms of security, and fraught with difficulties related to the weather vagaries and potential changes in vegetation and topography conditions [34]. The interaction of all these uncontrollable parameters and their combined effects on the fire itself can result in seemingly unpredictable behavior. Consequently, it is challenging to obtain repeatable conditions in the field because it is costly and difficult to achieve, especially for high intensity experimental fires. Thus, field-scale experiments are very valuable, especially relevant experimental data on high intensity fires that can be of primary interest in understanding the physical characteristics governing the behavior of such fires.

In this context, the main objective of this study is to present experimental fires carried out at field-scale on sloped terrains across dense and homogeneous shrubland vegetation, at different time periods (autumn and winter). The first field-scale fire was conducted in the north-western region of Corsica in October 2021, and the second in the south region of this island in March 2022. During these experiments, high intensity fires were obtained and all the detailed data concerning the propagation conditions collected in the sites can be used by the research community as a basis for comparison with numerical simulations carried out using different fire spread models. The experimental results obtained were compared with the numerical predictions provided by the fully physical fire model FireStar3D. This 3D approach was employed to assess the fire front dynamic, in particular the fire front speed and intensity. Results concerning the fire dynamics were also compared to predictions provided by the FireStar2D model. This model assumes an infinite fireline, which constitutes a thermal barrier that tends to deviate the air flow, whereas FireStar3D reproduces all the propagation conditions present in the real experimental fires, especially the limited fire front width composed by a succession of peaks and troughs that allows the air flow to cross and interact with the fire front. In addition, these experimental high-intensity fires were also analyzed in terms of fire front shape and flame tilt angle. Fire impact was also studied by evaluating radiant and total heat fluxes received by distant targets located at the end of the plot and comparing them with experimental measurements. Consequently, these comparisons highlighted the accuracy of this 3D computational model in predicting high intensity surface fire behavior and gave a better understanding of the fire propagation mechanisms across *Genista salzmannii* vegetation, and possibly other shrubland types that present similar physico-chemical properties.

In the next section the experimental method is described, followed by the modeling approach that was used. Then, the experimental and numerical results are detailed. Finally, an analysis and a discussion of the relevance and the significance of the obtained results are presented.

2. Materials and Methods

2.1. Experimental Protocol

Two field-fire experiments were conducted in different regions of Corsica across mountain shrubland plots (Figure 1a). The plot selection was based on two criteria that can generate high intensity fires close to wildfire conditions. The first is related to the terrain slope value where the average slopes of the selected sites were respectively 22° and 16°. The limits and the orientation of the plots were fixed according to the main

slope direction in order to favor high intensity fires. The second criterion is related to the structural homogeneity of the *Genista salzmannii* vegetation, with a high coverage >90%. The vegetation plots to be burned were in the shape of a rectangle (Figure 1b), about 30 m wide and 170 m long for the October experiment and 60 m long for the March experiment along the main slope direction. A common experimental protocol was used in these experiments to determine the propagation conditions related to the weather and topography and to characterize the physical properties of the vegetation. The focus of these experiments was on determining the behavior and impact of the high intensity fires. A brief description of this protocol will be presented next, while detailed information can be found in a previous article [35].

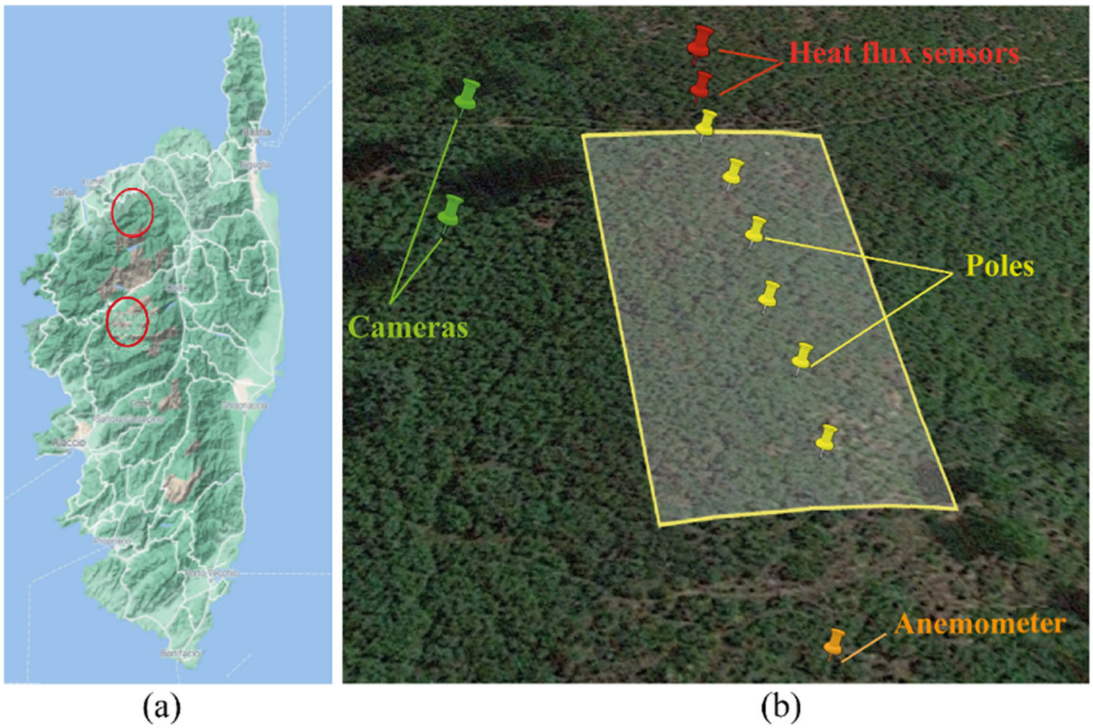

Figure 1. Experimental fire sites in Corsica island: (**a**) locations on the map (red circles); (**b**) view by Google earth and main GNSS measurement points during October 2021 experiment.

2.1.1. Characterization of the Vegetation and Weather Conditions

Thermochemical properties of the *Genista salzmannii* vegetation (Figure 2) can be found in the literature [36], while the physical properties which are dependent on the geographical area and weather conditions were evaluated onsite. Therefore, before the fire experiments, fuel sampling of fine fuel particles (diameters < 6 mm) was carried out in two areas of 1 m^2 in size in order to evaluate the total fuel load. In order to obtain the fuel moisture content, pre-fire samples of dead and live fine fuel particles were collected in double-sealed plastic bags. All samples were oven-dried for 48 h at a temperature of 60 °C. Fuel bed height was evaluated by averaging twenty different measurements of the distance between the top of the vegetation and the ground. The fuel volume fraction β was then obtained by calculating the ratio of the dry fuel load σ, the product of the particle density ρ_v and the average vegetation height e as given in Equation (1).

$$\beta = \frac{\sigma}{\rho_v \times e} \quad (1)$$

Figure 2. *Genista salzmannii* vegetation (October 2021 experiment site).

Concerning the ambient weather conditions, relative humidity and air temperature were monitored using a weather meter (Kestrel 5500, Kestrel Instruments, Boothwyn, PA, USA). In addition, a 2D ultrasonic anemometer (WS425, Vaisala Oyj, Vantaa, Finland) located at 3 m above the ground level was used to record the wind speed and direction acting on the fire front. Wind data were recorded using a data logger (CR3000, Campbell Scientific, Logan, UT, USA) at a sampling rate of 1 Hz. All parameters characterizing the vegetation and related to the meteorological and topographical conditions during the two experimental fires are listed in Table 1.

Table 1. Main average properties of *Genista salzmannii* vegetation and meteorological and topographical conditions.

	October 2021	**March 2022**
	Fuel Characteristics	
Fuel moisture content, FMC (%)	56	51
Fuel bed depth, e (m)	0.85	0.68
Dry fuel load, σ (kg/m^2)	1.79	2.67
Volume fraction, β	0.0021	0.004
Surface-area to volume ratio, s (m^{-1})	3100	
Particle density, ρ_v (kg/m^3)	970	
Fuel specific heat, Cp (J/kg/K)	1648	
Heat of combustion, ΔH_c (J/kg)	1.862×10^7	
	Meteorological and topographical conditions	
Average wind speed in the slope direction, U_3 (m/s)	1.3	1.3
Ambient temperature T (°c)	18	15
Relative humidity RH (%)	53	36
Terrain slope value (°)	22	16

2.1.2. Drones and Vision Technology for ROS Evaluation

During the experiment, fire front propagation was recorded from above using two drones in order to capture the fire spread from different positions, and from the sides by two cameras located on the ground. In order to simplify the video tracing, different poles were placed on reference equidistant points (Figure 1b). These points were used to evaluate the terrain slope value by determining their coordinates using a high-precision Global Navigation Satellite System (GNSS). They also allowed the evaluation of the rate of spread (ROS) by recording the time needed by the fire front to cross these reference poles when the fire reached a steady state propagation.

2.1.3. Heat Flux Measurements

In order to evaluate the impact of the fire front, the total and radiant heat fluxes were measured during the fire spread using 2 pairs of Medtherm transducers (16H and 64 Series, Medtherm Corp, Huntsville, AL, USA), located at different positions in a free vegetation area ahead of the plot (Figure 1b). Radiant and total transducers were oriented in the slope direction towards the fire, with view angles of 150° and 180°, respectively. The heat flux gauges were plugged into a power-supplied data logger (CR3000, Campbell Scientific) buried 0.3 m under the ground surface to protect it from fire. The extension cables were also buried into the ground up to the data logger and insulated by Teflon coating and aluminum foil (Figure 3). The transducer signals were recorded at a sampling rate of 1 Hz.

Figure 3. Radiant and total heat flux sensors fixed on supporting rod ahead of the vegetation plot and protected with aluminum foil.

2.2. Numerical Model

Numerical simulations were carried out using the fully physical fire model FireStar3D in order to test the relevance of numerical simulations in the case of high intensity fires. The results obtained in the 3D approach concerning the fire dynamic would then be compared to the experimental results, as well as to other numerical predictions given by a previous 2D version based on the same physical formulation (FireStar2D). The use of a 3D approach enabled us to render the 3D effects observed in real fires, and to present the heterogeneity of the fire front, forming a succession of peaks and troughs, allowing the wind flow to cross the fire front [37]. In contrast, in 2D the fire front is assumed to form a homogeneous obstacle, forcing the inlet wind flow to be deviated vertically with the convective plume which affects the interaction between the fire front and the vegetation layer [38–40]. Furthermore, the 2D model assumes an infinite ignition line, whereas in 3D it is possible to simulate a finite fire

front with the appropriate boundary conditions and their effects on fire front shape and behavior. For these reasons, numerical simulations using FireStar3D can reproduce more realistically the propagation conditions observed experimentally on the field.

The mathematical model used in FireStar3D is based on a multiphase formulation [41]. It involves locally averaging the conservation equations (mass, momentum, energy ...) governing the behavior of the coupled system formed by the vegetation and the surrounding atmosphere. This averaging is performed inside elementary control volumes including both the solid and the gaseous phases, inducing the introduction of some additional terms representing the interactions between the solid and the gaseous phase. Thus, this model consists of two parts, solved on two distinct grids. The first part consists of the equations related to the reacting turbulent flow in the gaseous phase, composed as a mixture of fresh air and gas products resulting from the solid phase degradation and the homogeneous combustion in the flaming zone. The second part consists of equations describing the decomposition of the solid phase subjected to the intense heat flux coming from the flaming zone.

Solving the gaseous phase model consists in the resolution of conservation equations of mass, momentum, energy (in an enthalpy formulation), and chemical species (O_2, N_2, CO, CO_2, and H_2O) filtered in space, using in this study a Large Eddy Simulation approach (LES), with a Favre average formulation [42]. The closure of the averaged conservation equations is based on the eddy viscosity concept [43] obtained from an evaluation of the turbulent kinetic energy k and its dissipation rate ε. In the case of the LES approach, a high-order sub-grid scale stress model is used [44]. The temperature dependence of the gas-mixture enthalpy is based on CHEMKIN thermodynamic tables [45]. In order to evaluate the combustion rate occurring in the gaseous phase, a combustion model based on Eddy Dissipation Concept (EDC) is used [46]. Finally, because radiation heat transfer plays an important role in the propagation of the fire front (mainly due to the presence of soot particles in the flame), the field of soot volume-fraction in the gas mixture is calculated by solving a transport equation [47] including a thermophoretic contribution in the convective term and taking into consideration soot oxidation [48].

Concerning the solid phase model, during thermal degradation, the composition of the solid fuel particles representing the vegetation is represented as a mixture of dry material (generic term for a mixing of cellulose, hemicellulose, and lignin), charcoal, moisture, and residual ashes. For each solid particle, the model consists of solving the equations governing the time evolutions of the mass fractions of water, dry material, and charcoal, as well as of the total mass of the solid particle, its volume fraction and its temperature (the model does not assume a thermodynamics equilibrium between the gas mixture and solid fuel particles). The degradation of the vegetation is governed by three temperature dependent mechanisms: drying, pyrolysis, and charcoal combustion. The pyrolysis process starts once the drying process is completed, and charcoal combustion starts once the pyrolysis process is achieved. The constants of the model associated with charcoal combustion (pre-exponential factor and activation energy) are evaluated empirically from a thermal analysis conducted on various solid fuel samples [41].

The interaction between the gaseous and the solid phases (exchanges of mass, drag, heat flux, etc.), is obtained through coupling terms that appear in both parts of the model. The details of the Firestar3D model have been thoroughly described in previous publications, where it was tested from calculations carried out at different scales for homogeneous fuel beds and was compared to experimental results as well as to empirical and semi-empirical models [37,49–51].

Simulations were provided using open boundary conditions on the two lateral sides of the computational domain as shown in Figure 4. The homogeneous vegetation layer, whose physical properties are given in Table 1, was 30 m wide in the y direction and 50 m long in the x direction. The domain inclination α was specified through two non-zero gravity components: $g_x = -g\ \sin(\alpha)$ and $g_z = -g\ \cos(\alpha)$, where $g = 9.81\ \mathrm{m/s^2}$ is Earth gravity. Initially (at t = 0), a one-seventh power horizontal velocity profile was imposed in

the entire computational domain with a 10-m open wind speed U_{10} = 1.54 m/s, and the hydrodynamic module of the code was run until reaching a statistically steady state. Once the flow had reached a statistically steady state, vegetation was ignited using a gaseous burner located along the entire leading edge of the vegetation layer. After burner activation, Neumann boundary conditions were applied at the inlet of the domain and a pressure gradient was automatically adjusted and imposed at the top of the domain to keep the velocity component in the Ox direction, at this position, equal to the initial value evaluated at t = 0. Concerning the mesh size, both the solid-phase and the fluid-phase grids were characterized by cells sizes below the radiation extinction length scale of the vegetation given by $4/s\beta$ [52,53], where s is the surface-to-volume ratio of the vegetation and β is the volume fraction of the solid phase. This value should not be exceeded in order to avoid fire extinction, especially in the case of radiation-dominated fire propagation.

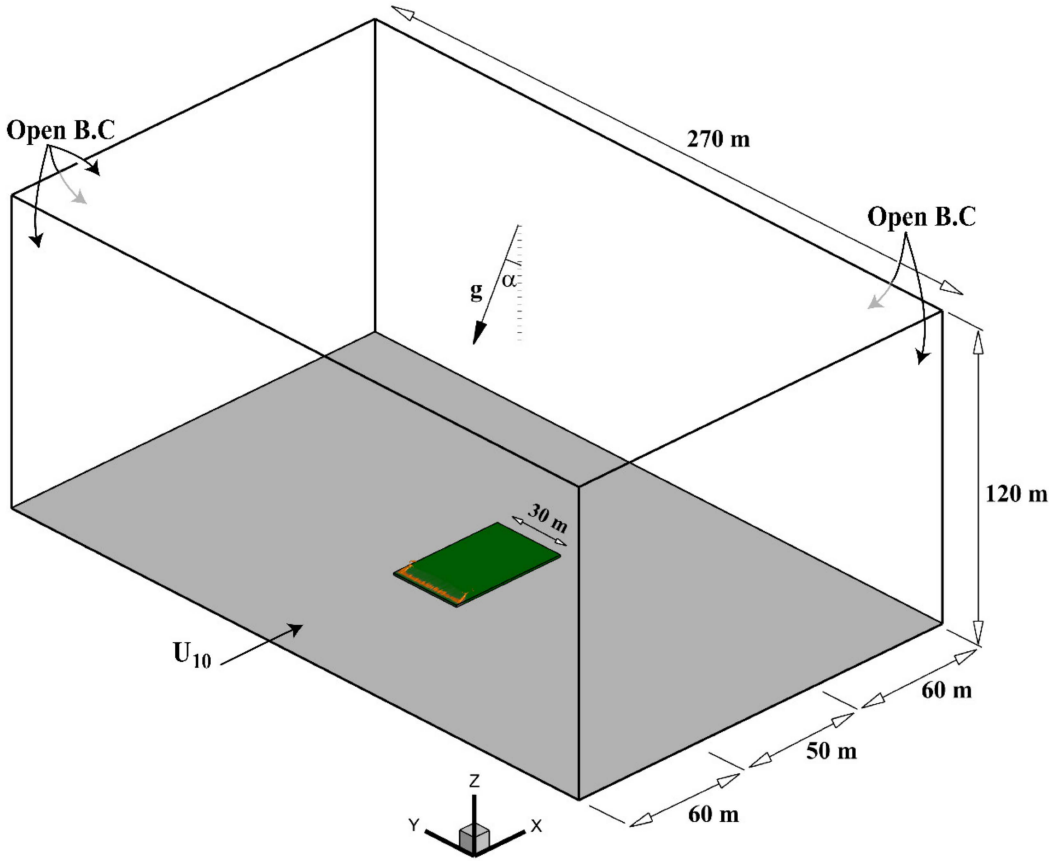

Figure 4. Perspective view showing the dimensions of the computational domain, the boundary conditions and the vegetation cover.

2.3. Evaluation Methods of Fire Behavior Parameters

The mathematical modelling of the wildland fires usually has two main objectives: firstly, the prediction of the fire dynamic related to the rate of spread and fire intensity, and secondly, the estimation of the fire impact related to the heat fluxes received at different positions. The evaluation methods of the parameters characterizing the fire behavior (ROS, fireline intensity, heat fluxes) are described in the following passage.

2.3.1. ROS

The experimental evaluation of the ROS as mentioned above is based on the time lapses taken by the fire to cross consecutive equidistant poles. Numerically, this parameter is obtained by calculating the time derivative of the pyrolysis front position at the fuel bed surface when the fire reaches a quasi-steady propagation.

2.3.2. Fireline Intensity

Fireline intensity represents a parameter that cannot be experimentally measured but only estimated through other measured quantities. There are different methods to evaluate this parameter at the center of the fire front where it reaches its maximum value. On the one hand, the experimental method is based on the ROS of the fire head, the heat of combustion of the vegetation ΔH_c, and the weight of the fuel consumed during the fire propagation $w_a = \mu\ \sigma$, where μ is the percentage of the fuel weight actually consumed in the active flaming front and effectively contributed to fire propagation [34] as given in Byram's intensity formulation (Equation (2)):

$$I_{BExp} = \Delta H_c \times w_a \times ROS \quad (2)$$

On the other hand, the numerical evaluation method using FireStar2D is based on the mass loss rate $\dot{m}$ of the vegetation due to dry material pyrolysis and charcoal combustion [54] (Equation (3)):

$$I_{BNum} = \dot{m} \times \Delta H_c \quad (3)$$

Using FireStar3D, fire intensity is estimated from the heat release rate *HRR* defined in the entire computational domain as given in Equation (4):

$$HRR = -\omega_{vap}\ \Delta H_{vap} - \omega_{pyr}\ \Delta H_{pyr} + \omega_{char}\ \Delta H_{char} + \omega_{CO}\ \Delta H_{CO} + \omega_{soot}\ \Delta H_{soot} \quad (4)$$

where ω_{vap}, ω_{pyr}, ω_{char}, ω_{CO} and ω_{soot} are respectively the total mass rates of water evaporation, pyrolysis, charcoal combustion, combustion of CO in the gas mixture, and soot combustion, and ΔH_{vap}, ΔH_{pyr}, ΔH_{char}, ΔH_{CO} and ΔH_{soot} are the corresponding heats of reaction [50].

The fireline intensity is estimated numerically by dividing the average value of the heat release rate when the fire is fully developed by the width w of the fire front [37,50] (Equation (5)):

$$I_{BNum} = \frac{HRR}{w} \quad (5)$$

2.3.3. Heat Fluxes

FireStar3D allows the evaluation of radiative and convective heat fluxes at any position in the computational domain. This permits to assess the radiative and total heat fluxes (equal to the sum of radiative and convective heat fluxes) recorded during the experiment by the fluxmeters located at the end of the plot. The details concerning the numerical evaluation of these heat transfer modes are presented in previous papers [35,37].

3. Results

3.1. ROS

Figure 5 shows the FireStar3D results for the time evolution of the most advanced point position of the pyrolysis front at the fuel bed surface. The corresponding ROS values, as well as experimental and 2D numerical values of ROS evaluated for both experiments, are given in Table 2.

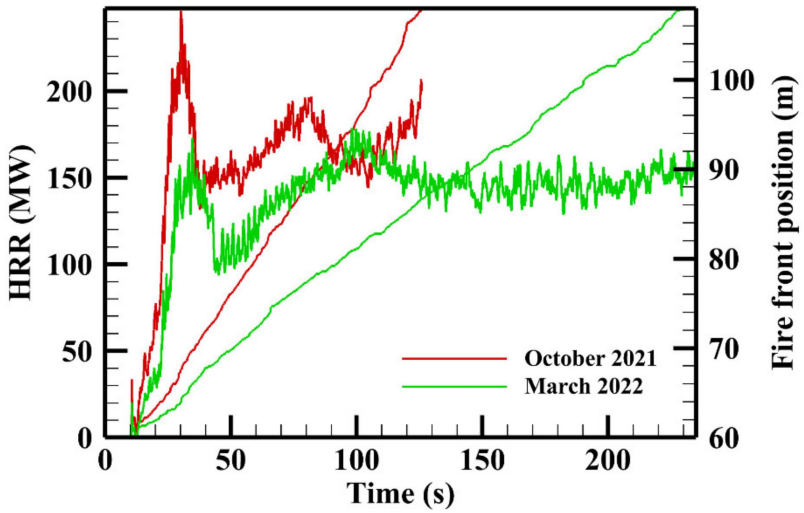

Figure 5. Variation with time of the fire front position as well as the heat release rate during the experiments conducted in October 2021 and March 2022, evaluated using FireStar3D.

Table 2. Experimental and numerical values of ROS and fireline intensity obtained using FireStar2D and FireStar3D.

	October 2021			March 2022		
	Experiment	**2D**	**3D**	**Experiment**	**2D**	**3D**
ROS (m/s)	0.38	0.47	0.41	0.21	0.29	0.20
Fireline intensity (MW/m)	12.7	9.9	8.4	10.4	9.5	7.1

3.2. Fireline Intensity

The time evolution of the heat release rates (Equation (4)) (until the fire fronts reached the end of the plots) evaluated in FireStar3D for both experiments is presented in Figure 6.

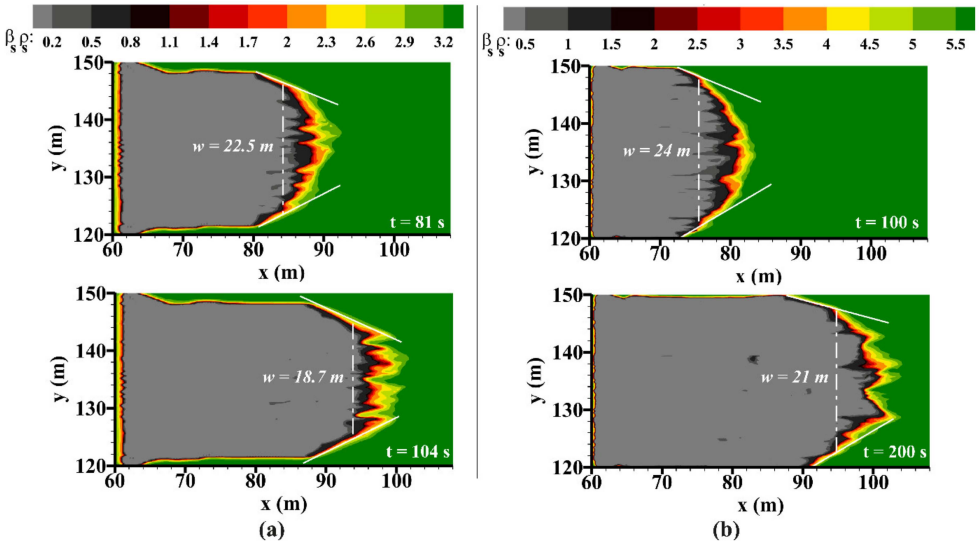

Figure 6. Distribution of the bulk fuel density at the top of the vegetation with the different width of the fire front head corresponding to the maximum and minimum heat release rates (HRR) evaluated for both experiments: (**a**) October 2021 (maximum HRR at t = 81 s; minimum HRR at t = 104 s); (**b**) March 2022 (maximum HRR at t = 100 s; minimum HRR at t = 200 s).

According to Equation (5) the fire front width must be estimated in order to calculate the fireline intensity value. For a fire front linearly moving with almost the same speed on

the whole perimeter length, w must be equal to the width of the computational domain. However, for both experiments, the limited length of a fire front propagating on a sloped terrain had a significant effect on a fire front behavior, creating a pointed fire front shape at the fire head [55]. Using open boundaries on the lateral sides of the domain permitted us to reproduce the real propagation conditions, and then obtain a parabolic fire front shape. In this case, w is assumed to be equal to the width of the most advanced part of the fire front head that contributes effectively to the maximum heat release rate. Fireline intensity is then evaluated by averaging the maximum and minimum values of the intensities, obtained at different simulation times as shown in Figure 6. Experimental and numerical values of fire intensities are listed in Table 2.

3.3. Flame Geometry and Fire Front Shape

The characteristics of the fire front geometry such as the flame length, height, and tilt angle are often quantities that provide insights into the fire dynamics [56,57]. The evaluation of these characteristics can also be very useful for firefighting operators in evaluating the impact of fire on a target [58,59] or the dimensioning of fuel breaks [60]. Flame characteristics have also been related to heat transfer during fire propagation [39] and also to the interaction of the fire with its environment, such as air entrainment capacity, which in turn affects fire behavior and flame geometry, particularly flame tilt angle [61].

In this study, flame tilt angle γ (Figure 7) was evaluated for the experiment of March 2022, using the videos recorded by a camera located at a lateral side of the plot. However, for the first experiment (October 2021), the visual estimation of the flame inclination angle using this method was not possible due to the heavy smoke generated by the fire. Figure 7 shows the experimental flame inclination angle γ evaluated between the bottom side of the visual flame and perpendicular to the ground that has an inclination angle of $\alpha = 16°$ from the red line representing a prefixed pole. The value of γ is then obtained by averaging seven different measurements leading to $\gamma = 40°$.

Figure 7. Visual estimation of the flame inclination angle for the experiment of March 2022.

In FireStar3D there is not yet a numerical method for the determination of the flame geometry. Thus, the flame inclination angle was estimated (averaged over several instants) geometrically from a hot gas isotherm of value equal to 1000 K, as shown in Figure 8. This threshold value (1000 K) was chosen because the temperature in the flame can vary between 1400 K at the base of the fire front and 700 K, which represents the limit temperature of the flame visibility [62]. Therefore, the average value of different tilt angles evaluated at several simulation times was equal to $\gamma = 54°$.

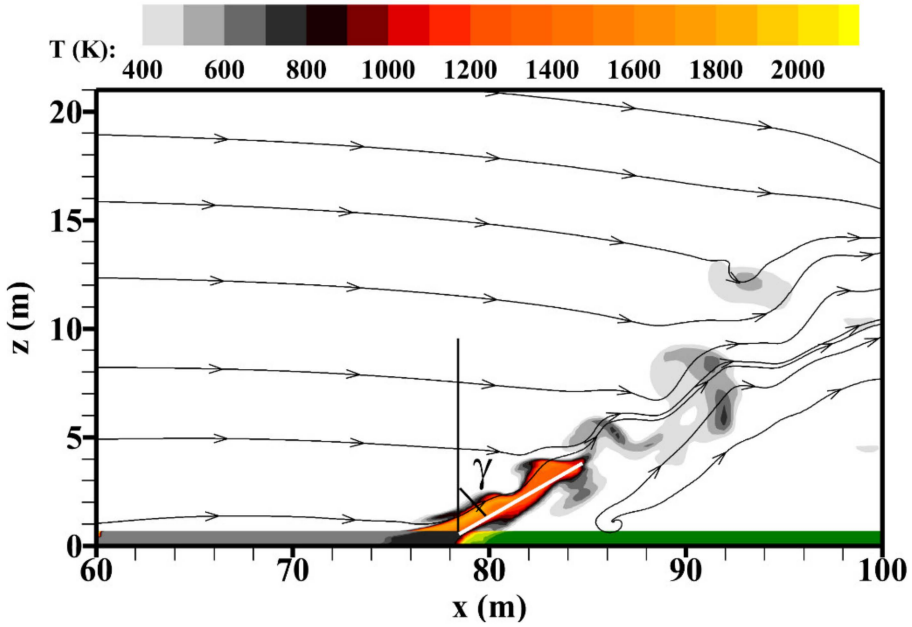

Figure 8. Flame inclination angle evaluated numerically using FireStar3D along the y-median plane and the streamlines of the gaseous phase, at a simulation time t = 120 s for March 2022 experiment.

As mentioned previously, fire front propagation was recorded from above using drones. IR images showed parabolic shapes of the fire front perimeter during these two fires spreading upslope, where the fire front head moved faster than the fire flanks (Figure 9).

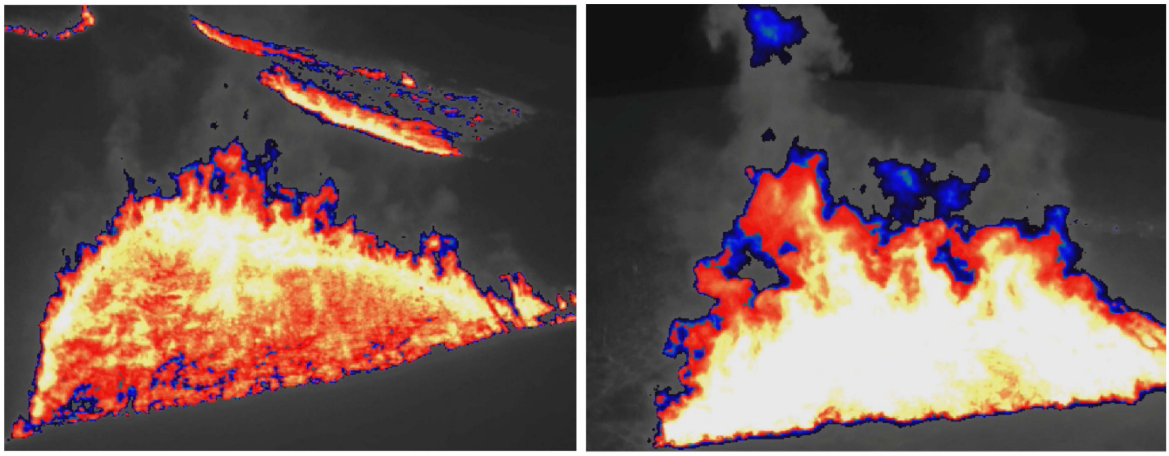

Figure 9. IR images captured from overhead drones during fire front propagation of the experimental fires performed in: (**a**) October 2021; (**b**) March 2022.

Numerical representations of the fire propagation obtained using Firestar3D showed almost the same curved head shapes (Figure 10), considering a limited fire front width with open boundary conditions on the two lateral sides, as was the real case during these two experimental fires.

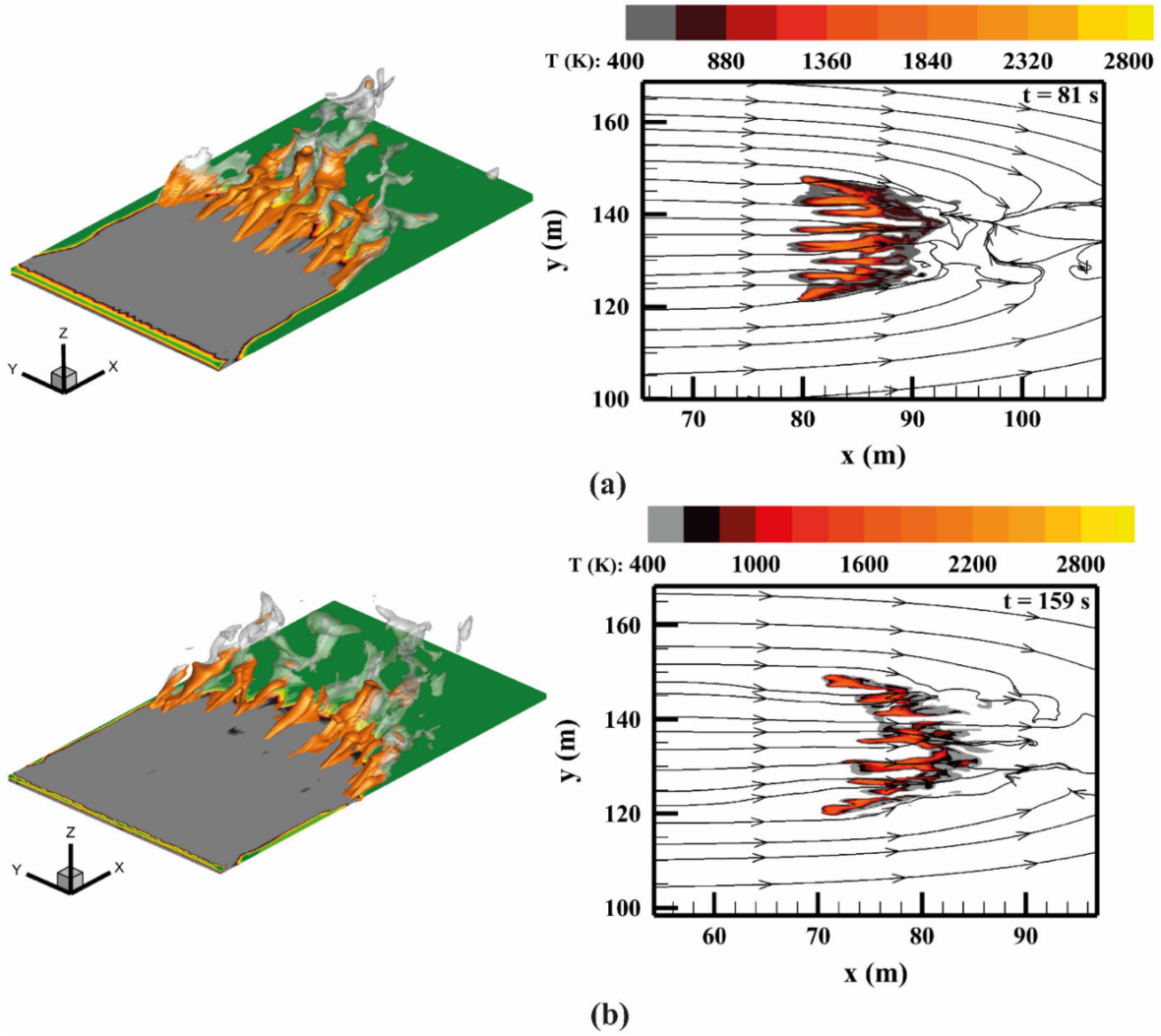

Figure 10. 3D evaluation of the fire front shape for an isotherm surface T = 1000 K (**left**), and a top view representing temperature fields and streamlines of the gaseous phase obtained in the horizontal plane (z = e (m)) (**right**): (**a**) October 2021; (**b**) March 2022.

3.4. Fire Front Impact

The fire impact was evaluated at different positions ahead of the fire front. Therefore, radiative and total heat fluxes received by the different transducers located at the end of the plots were recorded for both experiments. During the burn campaign in October, backfires conducted by the firefighters to protect the burning zone were close to the sensors, which affected the measurements during fire. In this case, only heat fluxes measured during the March experiment were investigated, and compared with numerical predictions.

Experimental heat fluxes received by the transducers were recorded during the experiment and the data analysis was carried out until the fire front reached the end of the plot. The targets were located at two positions, P1 and P2, as shown in Figure 11. Figure 12 shows the time evolution of the experimental radiative (Qr) and total (Qt) heat fluxes received by these two fluxmeters, while the numerical evaluation of these two heat transfer modes is reported in Figure 13. Figure 14 shows a better illustration in order to compare experimental and numerical radiative heat fluxes at both positions P1 and P2.

Figure 11. Positions P1 and P2 of the radiant and total fluxmeters with respect to the plot end (March 2022 experiment).

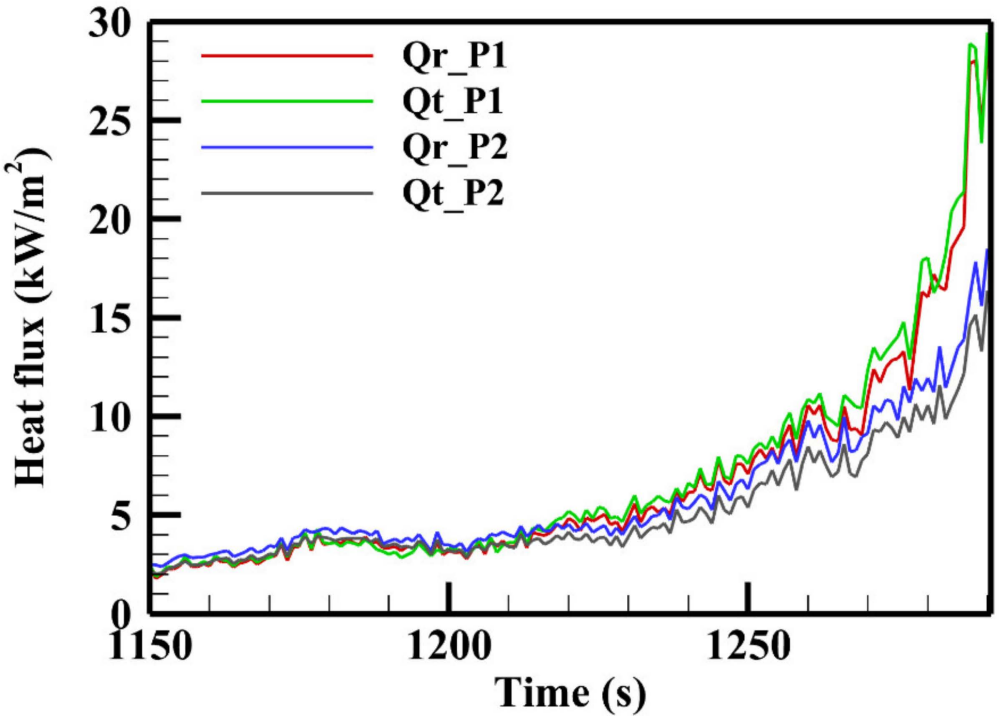

Figure 12. Time evolution of the radiative (Qr) and total (Qt) heat fluxes obtained experimentally at different target positions P1 and P2 during March (2022) experiment.

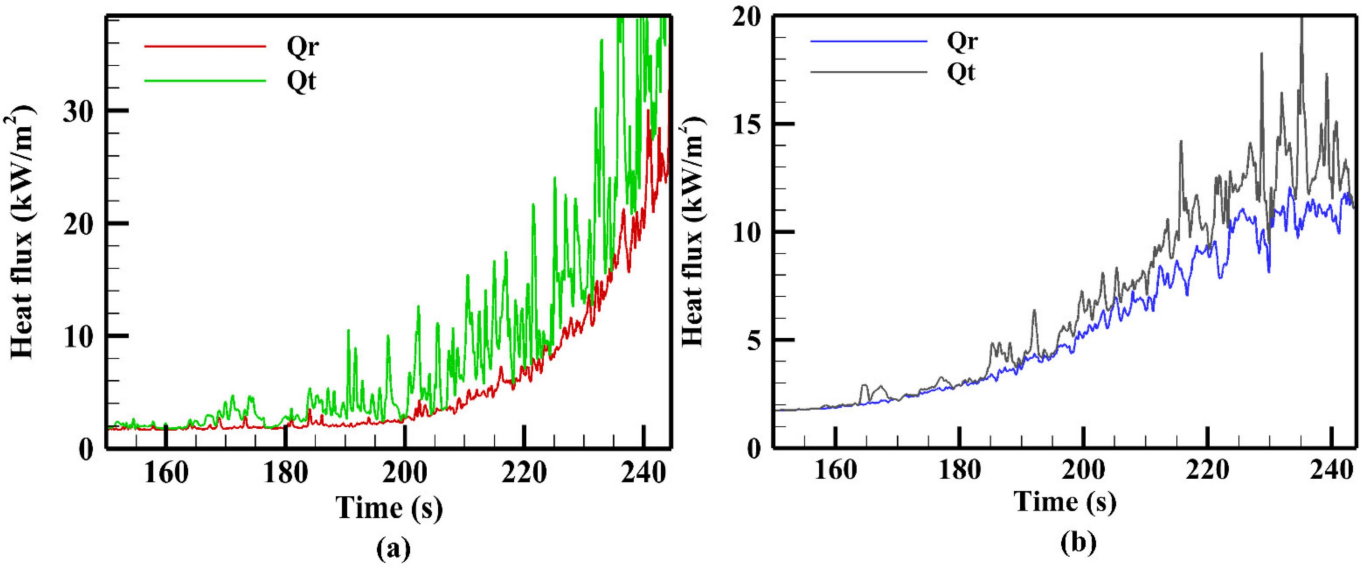

Figure 13. Time evolution of the radiative (Qr) and total (Qt) heat fluxes obtained numerically during March (2022) experiment at positions: (**a**) P1; (**b**) P2.

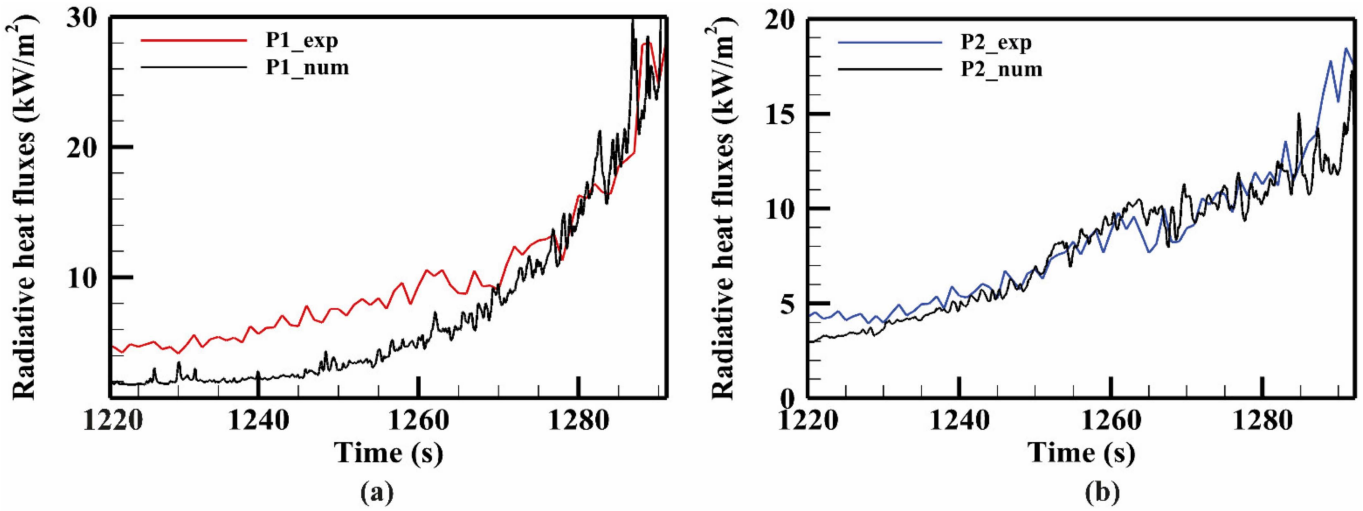

Figure 14. Time evolution of the radiative heat fluxes evaluated experimentally and numerically during March (2022) experiment at positions: (**a**) P1; (**b**) P2.

4. Discussion

4.1. Fire Front Behavior: ROS and Fireline Intensity

Numerical results concerning the ROS given by FireStar3D (Table 2) are in very good agreement with the experimental measurements with relative errors of 5.2% and 5% for both experiments. However, the predictions of ROS obtained by the 2D approach give errors of about 23.6% and 45%, with respect to the experimental results. The overestimation of the ROS given by FireStar2D may be due to different assumptions that are not present in the 3D approach. On the one hand, the 2D approach considers an infinite fireline propagating at the same speed across the entire width of the domain. On the other hand, in 2D model, the wind effect on the flame trajectory is overestimated because the flame is considered as a uniform thermal barrier that deviates the air flow vertically which tends to increase the flame inclination to the ground. For these reasons, heat transfer between the fire front and the unburned vegetation increases, and this may cause the overestimation of the ROS. In contrary, with FireStar3D, the open boundary conditions applied on both lateral sides of the domain with a finite fire front width induce lateral indrafts and cause the fire to slow

down near the sides. In this case, the leading point of the fire front remains in the central part throughout the simulation. In addition, the fire front structured as a succession of peaks and troughs allows for the air flow to find a way across it (Figure 10) [32,50] and to interact with the flames, which leads to a more accurate numerical representation of the fire propagation and behavior.

4.2. Fire Intensity

The results also estimate the fire line intensity, which is an index of the fire severity and the capacity of control [63]. Different rules have been developed to relate the fireline intensity to the suppression effectiveness [14,64]. The fireline intensity parameter is a quantity that cannot be measured but only estimated [65]. Using the experimental method to calculate this parameter (Equation (2)), the weight of the fuel consumed w_a is difficult to assess accurately due to the uncertainty of estimating the fuel load that contributes effectively to the fire front propagation during the combustion flaming stage. Fuel consumption is usually estimated as the difference between pre- and post-fire fuel inventories, which influences the estimation of fireline intensity [66]. For instance, for these experiments, w_a was supposed to be equal to the total dry fuel load because it represents only the load of the fine fuel particles (<6 mm) that were totally burned during experiments. Nevertheless, w_a must exclude post frontal smoldering which may continue for a long time after the front has passed [67]. It is known that there is less uncertainty in fuel types dominated by fine fuels such shrubs, where fine particles tend to limit the smoldering combustion behind the advancing flame front [65]. However, the amount of fuel consumed is affected by other parameters such as the fuel moisture content, especially when it exceeds 40% [68], and also the fuel volume fraction or packing ratio that plays a crucial role on the heat transfer between flame and vegetation inside the fuel bed, as well as on the fuel weight consumed [16]. For all these reasons, considering w_a to be equal to the total dry fuel load in the experimental evaluation may lead to an overestimation of I_{BExp}. Whatever the evaluation method of the fire intensity, the obtained numerical and experimental values refer to high intensity experimental surface fires, despite some unfavorable propagation conditions such as relatively high fuel moisture contents (56% and 51%) and low wind speeds (U_3 = 1.3 m/s). These fires can be extremely difficult to control in the case of real similar fire events, where the suppression actions must be restricted to the back and flanks of the fire because direct efforts to control the fire head are likely to fail [13,14].

4.3. Fire Front and Flame Geometry

Fireline shape development depends on the air entrainment activity into the flaming zone, especially the indrafts drawn by flames and the convection column from the lateral sides of the fuel bed in a direction not parallel to the propagation (Figure 10). If this mechanism occurs, the flow must converge towards the middle of the fuel bed for symmetry reasons [55], which explains why the head fire spreads more rapidly than the fire flanks, subjected to more deceleration in this case. For a high intensity fire propagating uphill under low wind speed conditions, as was the case in these two experimental fires, the lateral air entrainment becomes more important, and the fire induced wind from the burned zone behind the fire become stronger due to the presence of slope, which increases the fire front distortion into a pointed head shape. So, lateral air entrainment plays a key role in both the upslope fire front behavior and perimeter.

Concerning the flame inclination angle, this parameter depends on the balance between the horizontally moving ambient air and the buoyant velocity of the flame fluid [61,69]. For instance, as the slope angle increases, the flame tilt angle begins to increase significantly due to the influence of the fire induced wind. Thus, the flame height to depth ratio begins to decrease. The numerical modelling of these two mechanisms affecting the flame geometry can be subjected to some uncertainties, especially the upward flame buoyancy force related to the heat release rate. Therefore, due to the lower numerical

value of fireline intensity compared to the experimental one, a larger numerical value of flame tilt angle was then obtained.

4.4. Fire Front Impact

Concerning the fire front impact, Figures 12 and 13 reveal first that the experimental and numerical measurements have almost the same tendencies, with some numerical overestimation concerning the total (radiative and convective) heat flux parameter. Numerical fluctuations observed in the total heat fluxes concern the convective heat transfer mode, and are related to the velocity components used to evaluate the convective heat transfer coefficient. It should be noted that convective cooling has not been introduced into the numerical evaluation of the total heat fluxes received by the two fluxmeters. Nevertheless, both numerical and experimental results show a dominant contribution of the radiative heat transfer mode over these two transducers uphill from the fire.

Figure 14 shows almost the same levels and maximum values of radiative heat fluxes evaluated numerically and experimentally, when the fire front reaches the end of the plot. So, numerical predictions concerning the fire front impact were in fairly good agreement with the experimental measurements and could be used to estimate safety distances [58].

5. Conclusions

This paper reports two high intensity field-scale fires conducted on 22° and 16° sloped terrains during autumn and winter periods across Corsican shrubland vegetation. It describes the methodology used to obtain detailed collected measurements of the propagation conditions during experiments, and the numerical simulations of these two fires using the fully physical fire model FireStar3D. Fire behavior related to the ROS and fireline intensity was evaluated, and the numerical predictions show a good agreement with experimental results with a maximum difference of 5.2% for the head fire ROS. Despite some unfavorable propagation conditions such as the high fuel moisture contents (FMC > 56%) and the low wind speeds (U_3 = 1.3 m/s), fire intensities evaluated experimentally and calculated numerically for both fires were higher than 7 MW/m, which is representative of high intensity surface fires that can be very difficult to control in the case of similar wildfire events. Furthermore, additional parameters describing the fire front geometry were also investigated experimentally and numerically, such as the fire front contour and the flame inclination angle. Finally, the impact of fire on different targets located ahead of the fire front was measured experimentally and calculated numerically, and both results revealed almost the same tendencies, especially the dominance of the radiative heat transfer mode. Consequently, these comparisons lead to a better understanding of high intensity fires, and also show the robustness of the FireStar3D model to estimate high intensity surface fire behaviors and impacts across shrubland vegetation. Further studies on crown fires are planned in the future in order to better understand the different types of high intensity wildfires.

Author Contributions: Conceptualization, All the authors; methodology, J.-L.R., J.F., L.R. and F.M.; software, J.F., G.A., A.B., C.W. and L.R.; validation, All the authors; formal analysis, All the authors; writing—original draft preparation, J.F. and J.-L.R.; writing—review and editing, J.F., J.-L.R., F.-J.C., D.M. and S.M.; supervision, J.-L.R., F.-J.C., G.A. and D.M.; All authors have read and agreed to the published version of the manuscript.

Funding: This work was funded by the Corsican Collectivity and the French state in the framework of the collaborative project GOLIAT (CPER: 40031).

Institutional Review Board Statement: Not applicable.

Informed Consent Statement: Not applicable.

Data Availability Statement: Not applicable.

Acknowledgments: These field experiments required the cooperation of many people and would not have been possible without the assistance of the Departmental Fire Services of Corsica

(SIS2A and SIS2B) and the teams of the Corsican DFCI (Défense de la Forêt Contre l'Incendie) who selected the sites, constructed firebreaks, protected the areas, conducted the burning, and carried out fire suppression when spotting occurred. The authors really appreciated the collaboration with Jean-François Biancucci, member of the Regional Federation of Hunters of Corsica, who helped them select the second site. They would particularly like to thank the President of the SIS2A Véronique Arrighi who attended the experiment in March 2022.

Conflicts of Interest: The authors declare no conflict of interest.

Nomenclature

C_p	Fuel specific heat (J/kg/K)
e	Fuel bed depth (m)
g	Earth acceleration (m/s^2)
I_B	Byram fireline intensity (W/m)
I_{BExp}	Byram fireline intensity evaluated experimentally (W/m)
I_{BNUM}	Byram fireline intensity evaluated numerically (W/m)
FMC	Fuel moisture content (mass of water/mass of dry fuel)
ROS	Rate of spread (m/s)
s	Surface area to volume ratio (m^{-1})
T_0	Ambient temperature (K)
T	Gas mixture temperature (K)
T_a	Target temperature (K)
U_x	Wind speed at x meters above the ground (m/s)
ΔH_c	Fuel yield heat (J/kg)
w_a	Weight of fuel consumed in the active flaming front (kg/m^2)
$\dot{m}$	Vegetation mass loss rate (kg/m.s)
h_{conv}	Convective heat transfer coefficient (W/m^2.K)
k	Thermal conductivity of gas mixture (W/m.K)
B	Stephan-Boltzmann constant (W/m^2.K^4)
Pr	Prandtl number of gas mixture
R_e	Reynold number of fuel particles
Lc	Characteristic length (m)
$Qconv$, $Qrad$	Convective and radiative heat fluxes received by the target (W/m^2)
ΔH_{vap}, ΔH_{pyr}, ΔH_{char}, ΔH_{CO}, ΔH_{soot}	Enthalpy of water vaporization, pyrolysis, and charcoal, CO and soot combustion (kJ/kg)
ω_{vap}, ω_{pyr}, ω_{char}, ω_{CO}, ω_{soot}	Rates of water vaporization, dry material pyrolysis, and charcoal, CO and soot combustion (kg/s)
Greek	
ρ_v	Fuel particle density (kg/m^3)
β	Volume fraction of the solid phase
σ	Solid fuel load (kg/m^2)
γ	Flame inclination angle

References

1. European Science & Technology Advisory Group. *Evolving Risk of Wildfires in Europe—The Changing Nature of Wildfire Risk Calls for a Shift in Policy Focus from Suppression to Prevention*; UN Office for Disaster Risk Reduction: Brussels, Belgium, 2020.
2. European Commission, Directorate-General for Environment; Nuijten, D.; Onida, M.; Lelouvier, R. *Land-Based Wildfire Prevention: Principles and Experiences on Managing Landscapes, Forests and Woodlands for Safety and Resilience in Europe*; Nuijten, D., Onida, M., Lelouvier, R., Eds.; Publications Office of the European Union: Luxembourg, 2021; Available online: https://data.europa.eu/doi/10.2779/695867 (accessed on 15 December 2022).
3. Giorgi, F. Climate Change Hot-Spots. *Geophys. Res. Lett.* **2006**, *33*, 1–4. [CrossRef]
4. Mariotti, A.; Pan, Y.; Zeng, N.; Alessandri, A. Long-Term Climate Change in the Mediterranean Region in the Midst of Decadal Variability. *Clim. Dyn.* **2015**, *44*, 1437–1456. [CrossRef]
5. Russo, S.; Sillmann, J.; Fischer, E.M. Top Ten European Heatwaves since 1950 and Their Occurrence in the Coming Decades. *Environ. Res. Lett.* **2015**, *10*, 124003. [CrossRef]
6. Duane, A.; Castellnou, M.; Brotons, L. Towards a Comprehensive Look at Global Drivers of Novel Extreme Wildfire Events. *Clim. Chang.* **2021**, *165*, 43. [CrossRef]

7. Viegas, D.X.; Rossa, C.; Caballero, D.; Pita, L.P.C.; Palheiro, P. Analysis of Accidents in 2005 Fires in Portugal and Spain. *For. Ecol. Manag.* **2006**, *234*, S141. [CrossRef]
8. Molina-Terrén, D.M.; Xanthopoulos, G.; Diakakis, M.; Ribeiro, L.; Caballero, D.; Delogu, G.M.; Viegas, D.X.; Silva, C.A.; Cardil, A. Analysis of Forest Fire Fatalities in Southern Europe: Spain, Portugal, Greece and Sardinia (Italy). *Int. J. Wildland Fire* **2019**, *28*, 85–98. [CrossRef]
9. Li, M.; Shen, F.; Sun, X. 2019–2020 Australian Bushfire Air Particulate Pollution and Impact on the South Pacific Ocean. *Sci. Rep.* **2021**, *11*, 12288. [CrossRef]
10. Syphard, A.D.; Keeley, J.E.; Gough, M.; Lazarz, M.; Rogan, J.; Syphard, A.D.; Keeley, J.E.; Gough, M.; Lazarz, M.; Rogan, J. What Makes Wildfires Destructive in California? *Fire* **2022**, *5*, 133. [CrossRef]
11. Les Incendies Ont Causé Des Émissions de CO2 Records. Available online: https://reporterre.net/Les-incendies-ont-cause-des-emissions-de-CO2-records (accessed on 17 February 2023).
12. Balbi, J.-H.; Chatelon, F.J.; Rossi, J.L.; Simeoni, A.; Viegas, D.X.; Rossa, C. Modelling of Eruptive Fire Occurrence and Behaviour. *J. Environ. Sci. Eng. B* **2014**, *3*, 115–132.
13. Hirsch, K.; Martell, D. A Review of Initial Attack Fire Crew Productivity and Effectiveness. *Int. J. Wildland Fire* **1996**, *6*, 199–215. [CrossRef]
14. Tedim, F.; Leone, V.; Amraoui, M.; Bouillon, C.; Coughlan, M.R.; Delogu, G.M.; Fernandes, P.M.; Ferreira, C.; McCaffrey, S.; McGee, T.K.; et al. Defining Extreme Wildfire Events: Difficulties, Challenges, and Impacts. *Fire* **2018**, *1*, 9. [CrossRef]
15. Alexander, M.E. *Fire Behaviour as a Factor in Forest and Rural Fire Suppression*; Forest Research Bulletin No. 197; Forest and Rural Fire Scientific and Technical Series; Report No. 5; Forest Research, Rotorua, in association with the National Rural Fire Authority: Wellington, New Zealand, 2000.
16. Rothermel, R.C. *A Mathematical Model for Predicting Fire Spread in Wildland Fuels*; USDA Forest Service, Research Paper INT-115; Intermountain Forest and Range Experiment Station: Ogden, UT, USA, 1972.
17. Balbi, J.-H.; Rossi, J.-L.; Marcelli, T.; Chatelon, F.-J. Physical Modeling of Surface Fire Under Nonparallel Wind and Slope Conditions. *Combust. Sci. Technol.* **2010**, *182*, 922–939. [CrossRef]
18. Weise, D.R.; Koo, E.; Zhou, X.; Mahalingam, S.; Morandini, F.; Balbi, J.H. Fire Spread in Chaparral—A Comparison of Laboratory Data and Model Predictions in Burning Live Fuels. *Int. J. Wildland Fire* **2016**, *25*, 980–994. [CrossRef]
19. Catchpole, W.R.R.; Catchpole, E.A.A.; Butler, B.W.W.; Rothermel, R.C.; Latham, D.J.; Morris, G.A.; Latham, D.J. Rate of Spread of Free-Burning Fires in Woody Fuels in a Wind Tunnel. *Combust. Sci. Technol.* **1998**, *131*, 1–37. [CrossRef]
20. Rothermel, R.C.; Anderson, H.E. *Fire Spread Characteristics Determined in the Laboratory*; USDA Forest Service, Research Paper INT-30; Intermountain Forest and Range Experiment Station: Ogden, UT, USA, 1966.
21. Fang, J.B. *An Investigation of the Effect of Controlled Wind on the Rate of Fire Spread*; Department of Chemical Engineering, University of New Brunswick: Fredericton, NB, Canada, 1969.
22. Liu, N.; Wu, J.; Chen, H.; Zhang, L.; Deng, Z.; Satoh, K.; Viegas, D.X.; Raposo, J.R. Upslope Spread of a Linear Flame Front over a Pine Needle Fuel Bed: The Role of Convection Cooling. *Proc. Combust. Inst.* **2015**, *35*, 2691–2698. [CrossRef]
23. Awad, C.; Rossi, J.-L.; Marcelli, T.; Morvan, D.; Morandini, F.; Chatelon, F.-J.; Balbi, J.-H. Test of a Moisture Extinction Model under Conditions of No Slope and Calm Wind. In Proceedings of the 8th International Fire ecology and Management Congress, Tucson, AZ, USA, 18–22 November 2019.
24. Cheney, N.P.; Gould, J.S.; Catchpole, W.R. The Influence Of Fuel, Weather And Fire Shape Variables On Fire-Spread In Grasslands. *Int. J. Wildland Fire* **1993**, *3*, 31–44. [CrossRef]
25. Cruz, M.G.; Sullivan, A.L.; Gould, J.S.; Hurley, R.J.; Plucinski, M.P. Got to Burn to Learn: The Effect of Fuel Load on Grassland Fire Behaviour and Its Management Implications. *Int. J. Wildland Fire* **2018**, *27*, 727–741. [CrossRef]
26. Bilgili, E.; Saglam, B. Fire Behavior in Maquis Fuels in Turkey. *For. Ecol. Manag.* **2003**, *184*, 201–207. [CrossRef]
27. Anderson, W.R.; Cruz, M.G.; Fernandes, P.M.; McCaw, L.; Vega, J.A.; Bradstock, R.A.; Fogarty, L.; Gould, J.; McCarthy, G.; Marsden-Smedley, J.B.; et al. A Generic, Empirical-Based Model for Predicting Rate of Fire Spread in Shrublands. *Int. J. Wildland Fire* **2015**, *24*, 443–460. [CrossRef]
28. Antonio Vega, J.; Fernandes, P.; Cuiñas, P.; Fontúrbel, M.T.; Pérez, J.R.; Loureiro, C. Fire Spread Analysis of Early Summer Field Experiments in Shrubland Fuel Types of Northwestern Iberia. *For. Ecol. Manag.* **2006**, *234*, S102. [CrossRef]
29. Morandini, F.; Silvani, X.; Rossi, L.; Santoni, P.A.; Simeoni, A.; Balbi, J.-H.; Louis Rossi, J.; Marcelli, T. Fire Spread Experiment across Mediterranean Shrub: Influence of Wind on Flame Front Properties. *Fire Saf. J.* **2006**, *41*, 229–235. [CrossRef]
30. Silvani, X.; Morandini, F. Fire Spread Experiments in the Field: Temperature and Heat Fluxes Measurements. *Fire Saf. J.* **2009**, *44*, 279–285. [CrossRef]
31. Butler, B.; Teske, C.; Jimenez, D.; O'Brien, J.; Sopko, P.; Wold, C.; Vosburgh, M.; Hornsby, B.; Loudermilk, E. Observations of Energy Transport and Rate of Spreads from Low-Intensity Fires in Longleaf Pine Habitat-RxCADRE 2012. *Int. J. Wildland Fire* **2016**, *25*, 76–89. [CrossRef]
32. Raposo, J.; Viegas, D.X.; Xie, X.; Almeida, M.; Naian, L. A Dvances in F Orest F Ire R Esearch. In *Advances in Forest Fire Research*; Viegas, D.X., Ed.; Imprensa da Universidade de Coimbra: Coimbra, Portugal, 2014; pp. 88–94. ISBN 9789892608846.
33. Viegas, D.X. *Advances in Forest Fire Research 2018*; Coimbra University Press: Coimbra, Portugal, 2018. [CrossRef]
34. Byram, G.M. *Forest Fire Control and Use*; Davis, K.P., Ed.; McGraw-Hill: New York, NY, USA, 1959.

35. Fayad, J.; Rossi, L.; Frangieh, N.; Awad, C.; Accary, G.; Chatelon, F.-J.; Morandini, F.; Marcelli, T.; Cancellieri, V.; Cancellieri, D.; et al. Numerical Study of an Experimental High-Intensity Prescribed Fire across Corsican Genista Salzmannii Vegetation. *Fire Saf. J.* **2022**, *131*, 103600. [CrossRef]
36. Rahib, Y.; Leroy-Cancellieri, V.; Cancellieri, D.; Awad, C.; Rossi, J.-L. Comprehensive Characterization of Pyrolysis and Combustion of Genista Salzmannii Needles (GSN) for Fire Hazard Analysis. In Proceedings of the Advances in Forest Fire Research 2022; Viegas, D.X., Ribeiro, L.M., Eds.; Imprensa da Universidade de Coimbra: Coimbra, Portugal, 2022; pp. 1430–1436.
37. Morvan, D.; Accary, G.; Meradji, S.; Frangieh, N.; Bessonov, O. A 3D Physical Model to Study the Behavior of Vegetation Fires at Laboratory Scale. *Fire Saf. J.* **2018**, *101*, 39–52. [CrossRef]
38. Morvan, D.; Méradji, S.; Accary, G. Physical Modelling of Fire Spread in Grasslands. *Fire Saf. J.* **2009**, *44*, 50–61. [CrossRef]
39. Morvan, D.; Dupuy, J.L. Modeling the Propagation of a Wildfire through a Mediterranean Shrub Using a Multiphase Formulation. *Combust. Flame* **2004**, *138*, 199–210. [CrossRef]
40. Awad, C.; Frangieh, N.; Marcelli, T.; Accary, G.; Morvan, D.; Meradji, S.; Chatelon, F.-J.; Rossi, J.-L. Numerical Study of the Moisture Content Threshold under Prescribed Burning Conditions. *Fire Saf. J.* **2021**, *122*, 103324. [CrossRef]
41. Grishin, A.M. *Mathematical Modeling of Forest Fires and New Methods of Fighting Them*; Albini, F.A., Ed.; Publishing House of the Tomsk University: Tomsk, Russia, 1996.
42. Favre, A.; Kavasznay, L.S.G.; Dumas, R.; Gaviglio, J.; Coantic, M. *La Turbulence En Mécanique Des Fluides: Bases Théoriques et Expérimentales, Méthodes Statistiques*; Gauthier-Villars: Paris, France, 1977.
43. Cox, G. *Combustion Fundamentals of Fire*; Academic Press: London, UK, 1995; ISBN 9780121942304.
44. Gavrilov, K. *Numerical Modeling of Atmospheric Boundary Layer Flow over Forest Canopy*; Université de la Méditerranée–Aix Marseille II: Marseille, France, 2011.
45. Kee, R.J.; Rupley, F.M.; Miller, J.A. *The Chemkin Thermodynamic Data Base*; Sandia National Lab. (SNL-CA): Livermore, CA, USA, 1990.
46. Magnussen, B.F.; Hjertager, B.H. On Mathematical Modeling of Turbulent Combustion with Special Emphasis on Soot Formation and Combustion. In *Symposium (International) on Combustion*; Elsevier: Cambridge, MA, USA, 1977; Volume 16, pp. 719–729.
47. Syed, K.J.; Stewart, C.D.; Moss, J.B. Modelling Soot Formation and Thermal Radiation in Buoyant Turbulent Diffusion Flames. In *Symposium (International) on Combustion*; Elsevier: Cambridge, MA, USA, 1991; Volume 23, pp. 1533–1541.
48. Nagle, J.; Strickland-Constable, R.F. Oxidation of Carbon between 1000–2000 °C. In Proceedings of the Fifth Conference on Carbon; Elsevier: Cambridge, MA, USA, 1962; pp. 154–164.
49. Frangieh, N.; Morvan, D.; Meradji, S.; Accary, G.; Bessonov, O. Numerical Simulation of Grassland Fires Behavior Using an Implicit Physical Multiphase Model. *Fire Saf. J.* **2018**, *102*, 37–47. [CrossRef]
50. Frangieh, N.; Accary, G.; Morvan, D.; Méradji, S.; Bessonov, O. Wildfires Front Dynamics: 3D Structures and Intensity at Small and Large Scales. *Combust. Flame* **2020**, *211*, 54–67. [CrossRef]
51. Frangieh, N.; Accary, G.; Rossi, J.-L.; Morvan, D.; Meradji, S.; Marcelli, T.; Chatelon, F.-J. Fuelbreak Effectiveness against Wind-Driven and Plume-Dominated Fires: A 3D Numerical Study. *Fire Saf. J.* **2021**, *124*, 103383. [CrossRef]
52. Morvan, D. Physical Phenomena and Length Scales Governing the Behaviour of Wildfires: A Case for Physical Modelling. *Fire Technol.* **2011**, *47*, 437–460. [CrossRef]
53. Morvan, D.; Meradji, S.; Mell, W. Interaction between Head Fire and Backfire in Grasslands. *Fire Saf. J.* **2013**, *58*, 195–203. [CrossRef]
54. Morvan, D. Numerical Study of the Effect of Fuel Moisture Content (FMC) upon the Propagation of a Surface Fire on a Flat Terrain. *Fire Saf. J.* **2013**, *58*, 121–131. [CrossRef]
55. Dupuy, J.L.; Maréchal, J.; Portier, D.; Valette, J.C. The Effects of Slope and Fuel Bed Width on Laboratory Fire Behaviour. *Int. J. Wildland Fire* **2011**, *20*, 272–288. [CrossRef]
56. Rossi, J.L.; Simeoni, A.; Moretti, B.; Leroy-Cancellieri, V. An Analytical Model Based on Radiative Heating for the Determination of Safety Distances for Wildland Fires. *Fire Saf. J.* **2011**, *46*, 520–527. [CrossRef]
57. Rossi, J.-L.; Chetehouna, K.; Collin, A.; Moretti, B.; Balbi, J.-H. Simplified Flame Models and Prediction of the Thermal Radiation Emitted by a Flame Front in an Outdoor Fire. *Combust. Sci. Technol.* **2010**, *182*, 1457–1477. [CrossRef]
58. Zárate, L.; Arnaldos, J.; Casal, J. Establishing Safety Distances for Wildland Fires. *Fire Saf. J.* **2008**, *43*, 565–575. [CrossRef]
59. Page, W.G.; Butler, B.W. An Empirically Based Approach to Defining Wildland Firefighter Safety and Survival Zone Separation Distances. *Int. J. Wildland Fire* **2017**, *26*, 655–667. [CrossRef]
60. Rossi, J.-L.; Morvan, D.; Simeoni, A.; Marcelli, T.; Chatelon, F.-J. Fuelbreaks: A Part of Wildfire Prevention. In *Global Assessment Report 2019*; United Nations Office for Disaster Risk Reduction (UNDRR): Geneva, Switzerland, 2019; p. 25.
61. Nelson, R.M.; Butler, B.W.; Weise, D.R. Entrainment Regimes and Flame Characteristics of Wildland Fires. *Int. J. Wildland Fire* **2012**, *21*, 127–140. [CrossRef]
62. Wotton, B.M.; Gould, J.S.; McCaw, W.L.; Cheney, N.P.; Taylor, S.W. Flame Temperature and Residence Time of Fires in Dry Eucalypt Forest. *Int. J. Wildland Fire* **2012**, *21*, 270–281. [CrossRef]
63. Rossi, J.L.; Chatelon, F.J.; Marcelli, T. Fire Intensity. In *Encyclopedia of Wildfires and Wildland-Urban Interface (WUI) Fires*; Manzello, S.L., Ed.; Springer International Publishing: Cham, Switzerland, 2018; pp. 1–6. ISBN 978-3-319-51727-8.
64. Hirsch, K.G.; Corey, P.N.; Martell, D.L. Using Expert Judgment to Model Initial Attack Fire Crew Effectiveness. *For. Sci.* **1998**, *44*, 539–549. [CrossRef]

65. Alexander, M.E.; Cruz, M.G. Fireline Intensity. In *Encyclopedia of Wildfires Wildland-Urban Interface Fires*; Springer: Berlin/Heidelberg, Germany, 2020; pp. 453–460.
66. Alexander, M.E. Calculating and Interpreting Forest Fire Intensities. *Can. J. Bot.* **1982**, *60*, 349–357. [CrossRef]
67. Keeley, J.E. Fire Intensity, Fire Severity and Burn Severity: A Brief Review and Suggested Usage. *Int. J. Wildland Fire* **2009**, *18*, 116–126. [CrossRef]
68. Dahale, A.; Ferguson, S.; Shotorban, B.; Mahalingam, S. Effects of Distribution of Bulk Density and Moisture Content on Shrub Fires. *Int. J. Wildland Fire* **2013**, *22*, 625–641. [CrossRef]
69. Nelson, R.M. An Effective Wind Speed for Models of Fire Spread. *Int. J. Wildlands Fire* **2002**, *11*, 153–161. [CrossRef]